2018-01-1279 Published 03 Apr 2018

Curved Beam Based Model for Piston-Ring Designs in Internal Combustion Engines: Closed Shape Within a Flexible Band, Free-Shape and Force in Circular Bore Study

Mohamed Aziz Bhouri and Tian Tian Massachusetts Institute of Technology

Citation: Bhouri, M.A. and Tian, T., "Curved Beam Based Model for Piston-Ring Designs in Internal Combustion Engines: Closed Shape Within a Flexible Band, Free-Shape and Force in Circular Bore Study," SAE Technical Paper 2018-01-1279, 2018, doi:10.4271/2018-01-1279.

Abstract

A new multi-scale curved beam based model was developed for piston-ring designs. This paper describes the free-shape, force in circular bore and closed shape within a flexible band (ovality) related parts. Knowing any one of these distributions, this model determines the other two. This tool is useful in the sense that the characterization of the ring is carried out by measuring its closed shape within a flexible band which is more accurate than measuring its free shape or force distribution in circular bore. Thus, having a model that takes the closed shape within a flexible band as an input is more convenient and useful based on the experiments carried out to characterize the ring.

Introduction

Along with the cross-section and the running surface profile, ring free-shape is one of the geometry design key elements for top two rings [1, 2]. These elements determinate the ring sealing performances. Rings are also designed so that they conform well to bore distortions and create a liner force as uniform as possible in the circumferential direction under operation. To fulfill these requirements, ring free-shape has to be determined and manufactured within certain accuracy. Since the ring manufacturing process includes several operations, such as coating, that may modify the desired free-shape, this latter along with the radial pressure within bore have to be verified. Measuring ring closed shape within a flexible band is the most common procedure to determine ring pressure distribution. This measurement is carried out by enclosing the ring within a flexible band creating a constant pressure, different from the pressure distribution obtained within a circular bore. This non-direct correlation between the ring ovality and its radial pressure has been discussed in [3, 4, 5]. Our model presented in this paper shortcut this limitation via the four sub-models that determine the free-shape from the force distribution in circular bore or from the ring closed shape within a flexible band, and evaluate any of the two latter distributions from the free-shape (Figure 1). Therefore, we propose a method to relate any two of the three distributions (free-shape, closed shape within a flexible band and force in circular bore) from the third one.

Finite element methods have been used to model the structural behavior of the ring and its interaction with the cylinder [6, 7, 8, 9]. Cheng et al. [10,11] have recently developed a finite element ring-cylinder liner-piston groove contact model using eight-node hexahedral elements, providing a basis to carry out a 3D study of the ring-cylinder bore-piston interaction. Along with validating their model with experiments, they showed the importance of temperature gradient effect on the ring liner interactions and studied the sealing performance of positive twisted scraper second ring with negative ovality. However most of the existing structural model are based on straight beam model which has some limitations as the discontinuity of physical properties at the nodes of the finite element grid such as the curvature in addition to the large number of elements needed to reach sufficient accuracy which hamper the computation cost of these models. As proven by Baelden [12, 13], curved beam model resolved these issues.

A straight beam based ring design tool was developed by Liu [14]. Additionally, no model, whether based on curved or straight beam, determines the ring free shape and the force distribution in radial bore based on ring closed shape within a flexible band or any final ring shape given any arbitrary radial force distribution, which is carried out by the model we developed in this work. Moreover, conversions among ring's free shape, its closed shape within a flexible band and the force distribution in radial bore have not been done yet and will be useful for ring designer in order to facilitate the design process and minimize the number of iterations required to obtain the desired ring properties.

Our sub-model recovering the closed shape within a flexible band from the ring free shape relies on Euler-Lagrange equations with constant radial force. The sub-model that determines the force distribution in circular bore from ring

FIGURE 1 Free shape, force distribution in circular bore and closed shape within a flexible band (ovality) sub-modals representation.

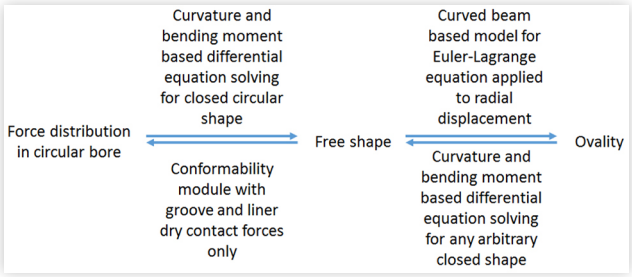

free shape simulates the ring inside the groove and cylinder with dry contact by adapting the conformability model developed within the ring design tool. Finally, the last two sub-models that determine the ring free-shape from the closed shape within a flexible band and force in circular bore distributions rely on a general theoretical framework built based on the differential equation satisfied by the ring free shape curvature and bending moment. Thus we define a complete tool that relates in any desired order these three ring's characterizations. For the conformability module used to recover the force distribution from the free shape, we deal with the ring closing process by considering initial loads needed to close the gap since small displacement assumption is not valid. For the other 3 sub-models, that assumption is violated so we use the general expression of the curvature for planar curve applied to the free shape and the closed one instead of the simplified expression.

As stated above, measuring the closed shape within a flexible band is more accurate than doing so for the free shape or force distribution in circular bore. Thus, the tool we developed is useful in the sense that having a model that takes the closed shape within a flexible band as an input is more convenient and useful based on the experiments carried out to characterize the ring.

A theoretical validation of these four models is presented by recovering the theoretical radial force distribution used first as an input and then recovered after being processed through all the four sub-models. The force distributions (Usual/Standard and TC) are provided by Mahle and were studied by Tomanik [15]. The TC ring (called TC1 in [15] and TC in this paper) is a design proposed by Mahle to minimize the contact pressure at the ring tips during engine operation. The corresponding optimized pressure distribution follows a more complex equation such that the tip pressure, under static conditions, is usually set to zero. A validation of the model using measurements of closed shape within a flexible band is also presented and limitation of the results is also discussed. These measurements were also provided by Mahle for the same ring considered in the theoretical validation. For the simulations carried out with the measurements as input, we were able to recover the theoretical free shapes, but not the corresponding theoretical force distributions. Nevertheless, we investigated the reasons behind it and gave an initial explanation.

Determining Ring's Force Distribution in Circular Bore Using Its Free Shape

Determining the ring force distribution in circular bore using its free shape is carried out using the conformability module developed for the curved beam based ring design tool by considering only dry contact forces from the groove and the liner. A dual grid curved beam finite element method was developed by Baelden [12, 13] first and then used by Y. Liu [16, 17, 18] to successfully assemble a multi-scale-length ring pack model that provides an accurate description of a cycle model and all the relevant mechanisms taking part in it within a reasonable computation cost.

This curved beam finite element method takes advantage of the dual grid used for the ring's deformations and the contact force based on the typical length scales they rely on. Ring structural deformations are solved with sufficient accuracy using a coarse structural mesh and local interactions are studied based on a much finer grid.

The radial and axial displacement of the ring neutral axis are interpolated using 5th order Hermite polynomial spline in order to guarantee the continuity of these displacements up to their second derivative. Hence, under the small displacement assumption, the continuity of the curvatures corresponding to the radial and axial displacement, which is the key variable for bending, follows as we can see in equations (1)-(3) where R is the nominal ring radius, y the radial displacement, z the axial lift and α the angle between the principal frame and cylindrical one as shown in Figure 2.

$$\kappa = \frac{1}{R} - \frac{y + y''}{R^2} \tag{1}$$

$$\kappa_{yy} = \kappa \cos\left(\alpha + \frac{z''}{R}\right) \tag{2}$$

$$\kappa_{zz} = \kappa \sin\left(\alpha + \frac{z''}{R}\right) \tag{3}$$

FIGURE 2 Ring principle frame (blue), Natural frame (red) and Cylindrical frame (green).

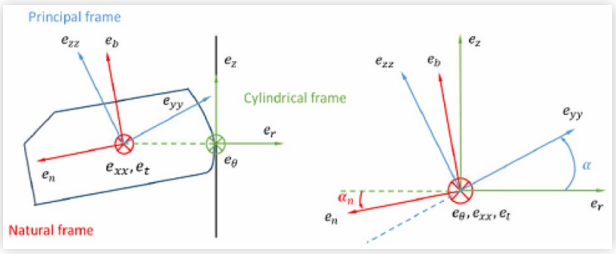

The expressions of the different bending moments and twist moment are given below (4)-(6) and show the dependence on the ring coordinates and their derivatives, where E is ring Young modulus, I_{zz} its cross section moment of inertia in plane, I_{yy} its cross section moment of inertia out of plane, J_t its torsion factor and its shear modulus. κ_{yy0} and κ_{zz0} refer to the ring free-shape curvature corresponding to the radial and axial projections.

$$M_{zz} = EI_{zz}\left(\kappa_{yy} - \kappa_{yy0}\right) \tag{4}$$

$$M_{yy} = EI_{yy}\left(\kappa_{zz} - \kappa_{zz0}\right) \tag{5}$$

$$M_{\theta} = GJ_t\left(\frac{z' - R\alpha'}{R^2}\right) \tag{6}$$

Since the twisting moment depends on the first derivative of the twist angle and its second derivative does not appear in the expressions of the different moments, a 3rd order polynomial interpolation is sufficient and requires only ring twist and its first derivative at the nodes.

Next we apply Hamilton's principal by considering Euler-Lagrange equations and introduce an intermediate state in our simulation which corresponds to closing the ring from its free-shape to the circular bore. During that process the small displacement assumption is violated and hence the simplified expressions of the curvature and moments provided above are not valid anymore. The closing process is considered by taking into account the load required to close the ring from its free-shape as an initial one.

The finite element equation of motion is derived for each element. Then, the different element matrices and vectors are assembled to obtain the finite element equations of the complete ring with global matrices. More details can be found in M.A. Bhouri thesis [19].

Determining Ring's Free Shape Using Its Force Distribution in Circular Bore

The ring free shape is a key characterization of the ring. In practice, designers need to determine the geometry of the ring free shape that will produce the desired ring tension and force distribution once the ring is closed to the bore diameter. The following model lets us recover the ring free shape from known force distribution along the ring circumference in circular bore.

To compute the ring free shape, we determine first its curvature. To do so we use the bending moment equation (4) along the axial direction which is proportional to the curvature change in the radial one. We keep using the same notations introduced previously.

$$M_{zz} = EI_{zz}\left(\kappa_{yy} - \kappa_{yy0}\right) \tag{4}$$

FIGURE 3 Bending moment and radial force distribution.

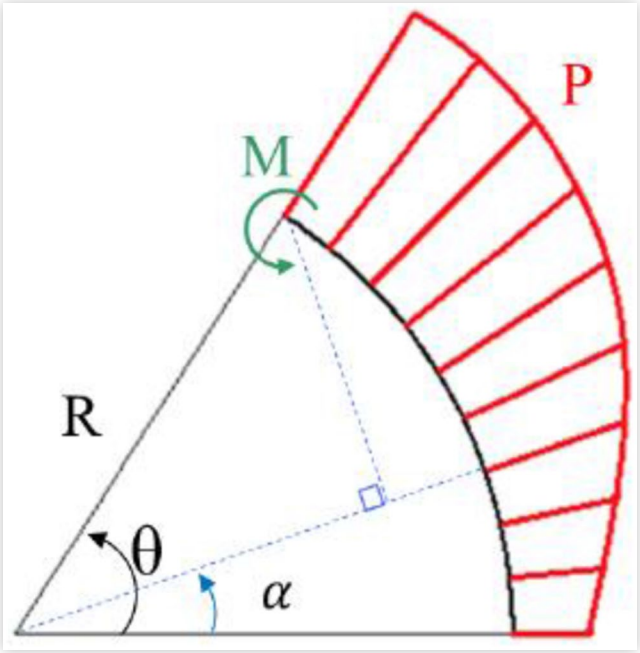

κ_{yy} is the the curvature of the closed ring while κ_{yy0} is the free shape curvature. Since the final shape is a circular one, $\kappa_{yy} = \frac{1}{R}$.

The bending moment (Figure 3) is calculated from the force distribution starting from the ring gap $\theta = 0$ which is a free end without any internal or external stress.

For planar curve, we can express the ring free shape curvature as follows:

$$\kappa_{yy0} = \frac{r_{fs}^2 + 2r_{fs}'^2 - r_{fs}r_{fs}''}{\left(r_{fs}^2 + r_{fs}'^2\right)^{\frac{3}{2}}} \tag{7}$$

$$r_{fs} = R + y_0 \tag{8}$$

r_{fs} is the radius of the ring free shape. We solve the differential equation in the arc length coordinate system s along with the boundary conditions imposed at the back of the ring.

The ring free shape curvature can be computed directly from the bending moment without solving any differential equation which gives more accurate results than evaluating the curvature from the solution obtained for the ring free shape r_{fs} based on (7). This is of utmost importance since when using the free shape as input to any of our models, either to determine the force in circular bore or the closed shape within a flexible band distribution, all we need to use is the curvature which appears in the resulting Euler-Lagrange equations in each case (that term is inserted in the initial load vector in our conformability module that we use to determine the force distribution in circular bore) and once we know the curvature we don't need to use neither the ring free shape r_{fs} nor its first or second derivatives. More details can be found in M.A. Bhouri thesis [19].

Determining Ring's Closed Shape Within a Flexible Band Using Its Free Shape

Given a certain ring design, by applying a certain constant pressure on it we can make its gap closed. We call the final shape obtained afterwards ovality distribution or closed shape within a flexible band distribution. We also use this name to design the final shape obtained after applying a constant radial pressure on the ring whether the gap is perfectly closed or not, but by specifying its value in the latter case.

To determine the closed shape within a flexible band distribution from the free shape, we can solve the Euler-Lagrange equations since we are looking at the final static state of the ring. Therefore, the finite element curved beam model can be used. In this case, we only have the strain energy related to in plane bending. The work of external contains only the constant radial force. We use 5th order spline interpolation for radial displacement along with the Hamilton's principle to obtain the Euler-Lagrange equations for each ring element. In order to obtain the finite element equations for the complete ring, we assemble the terms obtained for the different ring elements. We end up with a non-linear system that we solve using Newton-Raphson algorithm. More details can be found in M.A. Bhouri thesis [19].

Determining Ring's Free Shape Using Its Closed Shape Within a Flexible Band

Determining the ring free shape from its closed shape within a flexible band is a generalization of the process described in section - Determining ring's free shape using its force distribution in circular bore - where we determined the ring free shape from the force distribution in circular bore. In this section, we derive the equation to be solved in order to determine the free shape from any closed shape with any pressure distribution applied to it.

To compute the ring free shape, we determine its curvature using the bending moment equation (4) along the axial direction. The difference with the circular shape is in the integral expression of the local bending moment (Equations 9 and 10 and Figure 4). $P(\alpha)$ is the contact pressure distribution applied on the ring when it is closed to the final shape. α is the angle swiping from 0 to θ.

$$M_{zz} = EI_{zz}\left(\kappa_{yy} - \kappa_{yy0}\right) \tag{4}$$

$$M_{zz} = \int_0^{\theta} P(\alpha)\, r_{ov}(\alpha)\, f\left(r_{ov}(\alpha), \alpha, \theta\right) d\alpha \tag{9}$$

FIGURE 4 Bending moment and radial force distribution for any arbitrary closed shape.

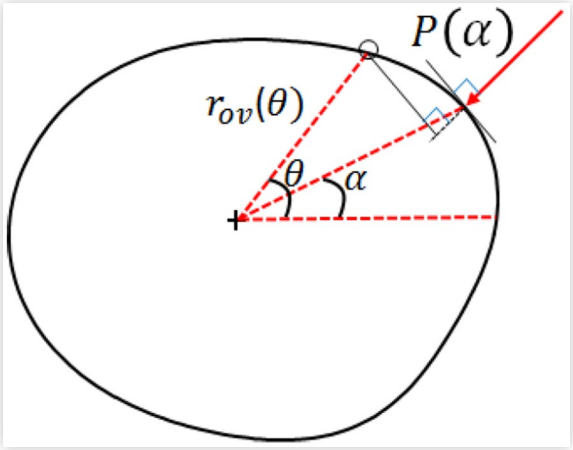

$$f\left(r_{ov}(\alpha), \alpha, \theta\right) = \frac{\left|\begin{array}{l}\left(r'_{ov}(\alpha)\cos(\alpha) - r_{ov}(\alpha)\sin(\alpha)\right) r_{ov}(\theta)\cos(\theta) + \\ \left(r'_{ov}(\alpha)\sin(\alpha) + r_{ov}(\alpha)\cos(\alpha)\right) r_{ov}(\theta)\sin(\theta) - r_{ov}(\alpha) r'_{ov}(\alpha)\end{array}\right|}{\sqrt{\left(r'_{ov}(\alpha)\cos(\alpha) - r_{ov}(\alpha)\sin(\alpha)\right)^2 + \left(r'_{ov}(\alpha)\sin(\alpha) + r_{ov}(\alpha)\cos(\alpha)\right)^2}} \tag{10}$$

κ_{yy} is the curvature of the closed ring (11).

$$\kappa_{yy} = \frac{r_{ov}^2 + 2r_{ov}'^2 - r_{ov}r''_{ov}}{\left[r_{ov}^2 + r_{ov}'^2\right]^{\frac{3}{2}}} \tag{11}$$

We solve the differential equation in the arc length coordinate system s along with the boundary conditions imposed at the back of the ring.

The ring free shape curvature can be computed directly from the bending moment without solving any differential equation to obtain more accurate results. As stated before, this is useful since when we will use the free shape results as input to another sub-model, all we need is its curvature. More details can be found in M.A. Bhouri thesis [19].

Validation of the Four Models

In this section we present a theoretical validation of the four models based on data provided by Mahle. We have two different data sets for the same ring of rectangular cross section with a radial width equal to 4 *mm* and an axial one equal to 2 *mm*. The nominal radius at the compressed state is of 45.625 *mm*. Each data set corresponds to a certain pressure distribution and therefore to specific closed and free shapes.

Tomanik presented a theoretical study and experimental procedure to characterize the free and closed shapes of these two ring types [15]. We call these data sets by the Usual and the TC one, using the same nomenclature given to the rings. The force distribution (force per ring axial width) for each of them is plotted in Figure 5. The Usual ring pressure distribution follows a 2nd order harmonic, while the TC optimized pressure is set to zero at the ring tips, under static condition. When closed, the gap clearance for the Usual case is equal to 0.48 *mm*, while it is 0.4 *mm* for the TC one.

In order to validate theoretically the four models introduced previously, we start with these force distributions to compute the corresponding free shapes and then the closed shapes within a flexible band. Then, we recover again the free shapes and force distributions. For each of the four steps we use the appropriate sub-model presented above. Based on Figure 1 this is equivalent to going from left to right and then in the opposite direction.

As stated above, at any time we compute the ring free shape, we keep the curvature computed from the relation based on the bending moment and not from the expression based on the radial coordinates of the ring free shape which involves first and second derivatives. We will also compare the free shape and its curvature computed from the force distribution and from the closed shape.

All our models rely on the usual representation for the free shapes. It means that the radial coordinates are computed as the distance between the ring points and the center of the circle adjacent to the ring back free-shape with a radius equal to the ring nominal radius. Mahle data sets are available in the centralized representation where the radial coordinates are defined as the distance between the ring points and the center of the circle passing through the ring back and the tips.

Figure 6 shows the closed shape within a flexible band obtained from the theoretical pressure distribution for the usual case in radial coordinates and its comparison with the measured one using the centralized representation. Figure 7 provides the same results for the TC case. In the sub model

FIGURE 5 Theoretical radial force distribution for usual and TC cases.

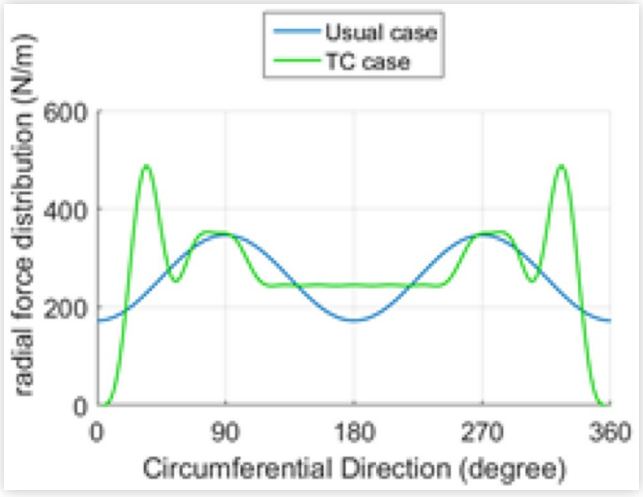

FIGURE 6 Closed shape within a flexible band obtained from theoretical force distribution compared to the measured one in centralized representation (Usual case).

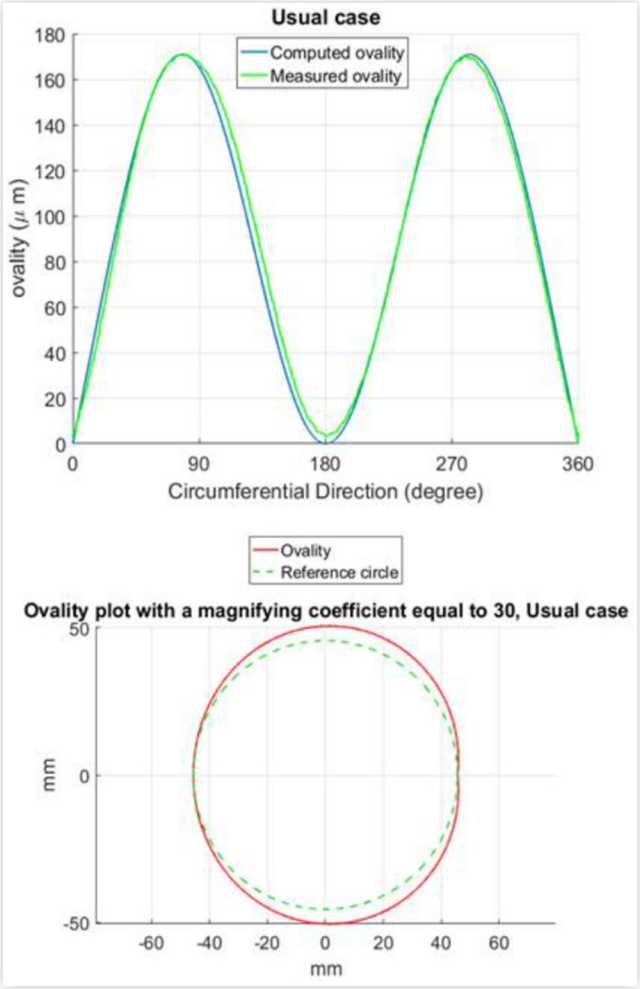

computing the closed shape within a flexible band from the free shape, we use 16 elements. A sensitivity analysis was carried out to verify that this number of elements is adequate for our calculation and that the results vary only very slightly when we increase it.

Figures 8 and 9 show the results obtained for the free shapes in the usual representation at two different steps: when computed from the theoretical force distribution and when determined from the closed shape within a flexible band computed by our models. We notice that our models are consistent since they recover the same free shape for each case. We obtained a maximum relative error between the two free shapes of 0.6% for the two cases.

In figures 10 and 11, we compare three different free shape curvatures. The dashed green one corresponds to the free shape curvature obtained from the theoretical force distribution using its relation with the bending moment. The blue curve is the free shape curvature computed from the momentum equation (4) applied to the closed shape within a flexible band computed in our model. Finally, the dashed red curve shows the free shape curvature computed using

FIGURE 7 Closed shape within a flexible band obtained from theoretical force distribution compared to the measured one in centralized representation (TC case).

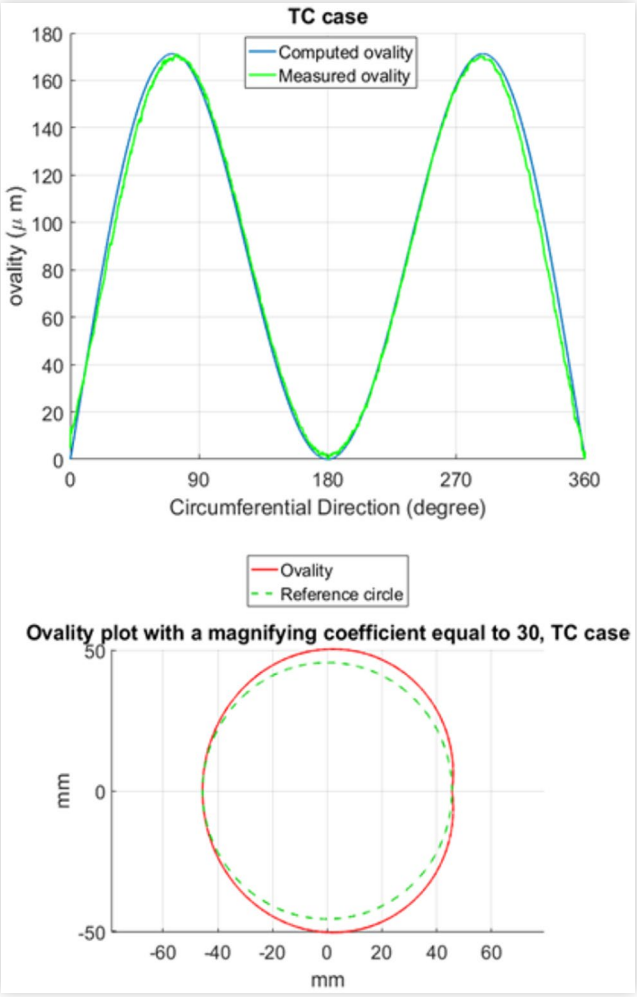

FIGURE 8 Comparison of free shape obtained from theoretical force distribution and from computed closed shape within a flexible band in usual representation (usual case). The black dashed line shows the circle with nominal radius.

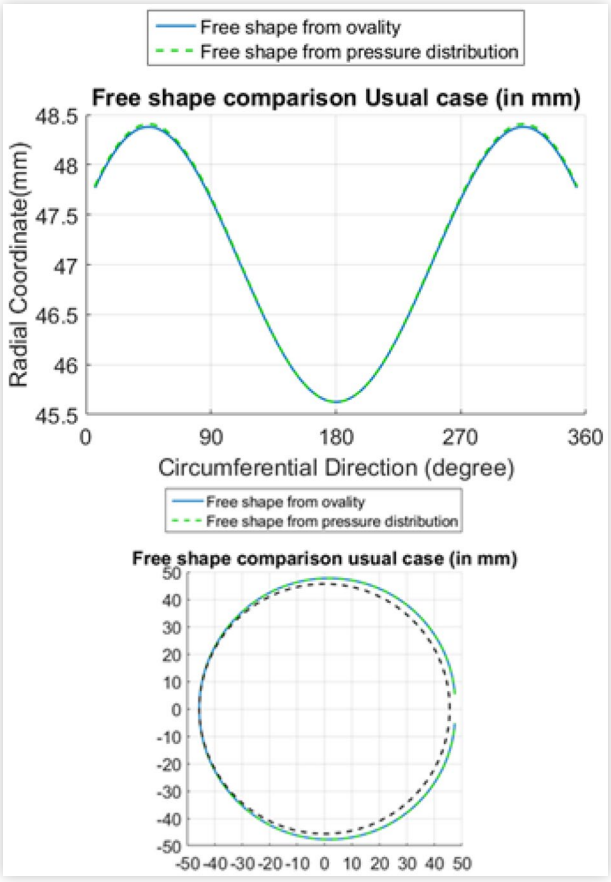

equation (7) after solving for the ring free shape radial coordinates using the closed shape within a flexible band computed in our model. Again our models are all consistent and provide the same results for the curvature for both the usual and the TC cases. For the usual case, we obtain a maximum relative error of 0.02% for the curvature computed from the momentum equation and an error of 0.07% for the one computed using the free shape radial coordinates. For the TC case, we obtain a maximum relative error of 0.03% for the curvature computed from the momentum equation and an error of 0.08% for the one computed using the free shape radial coordinates.

Finally, we retrieve the force distribution in closed circular shape using the free shape curvature computed from the closed shape that we determined. We use the free shape curvature determined using the momentum equation (4) based on the closed shape (curvature in blue curve in Figures 10 and 11). The results are presented in Figures 12 and 13. In the last sub model computing the force distribution from the free shape, we use 16 elements and 1000 points per element. A sensitivity analysis was carried out to verify that the chosen number of elements and points are adequate for our calculation and that the results vary only very slightly when we increase any of them.

As stated above, the force distribution is taken as the force applied from the liner on the ring. The contact model adopted, the roughness of the liner and its material related properties explain the small differences we observe in the two force distributions since the provided ones are theoretical and independent from the source applying it on the ring.

As a conclusion, our four sub models are consistent all together and able to recover the inputs we provide them with by determining any two variables from the third one among the ring free shape, its closed shape within a flexible band and the force distribution in closed circular shape. However, our models showed some limits when we tried to validate them with experimental measurements. More details are provided in the following section along with some explanations regarding the discrepancies observed which are not only related to our models but also to the measurement deviations.

FIGURE 9 Comparison of free shape obtained from theoretical force distribution and from computed closed shape within a flexible band in usual representation (TC case). The black dashed line shows the circle with nominal radius.

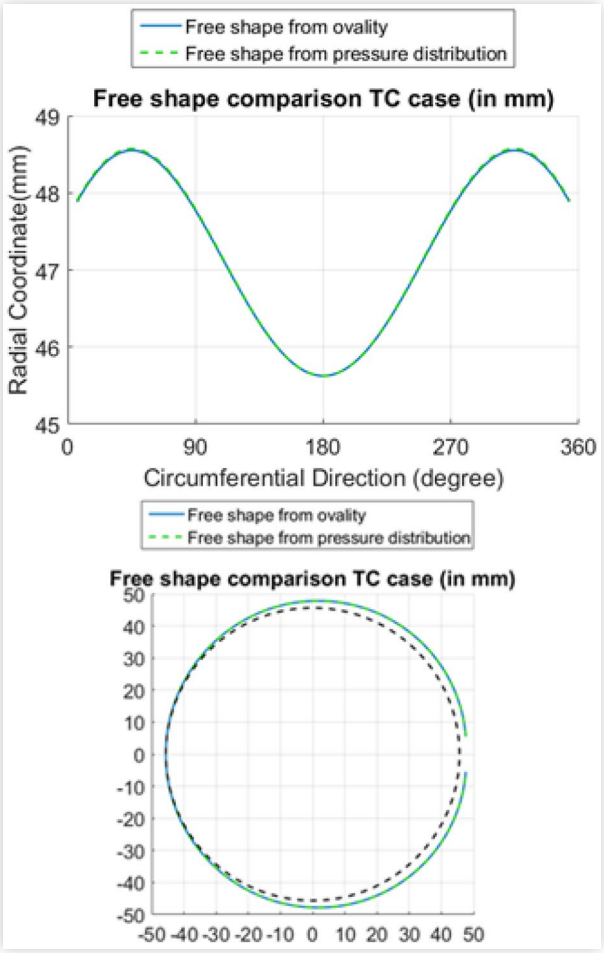

FIGURE 10 Free shape curvature comparison (Usual case).

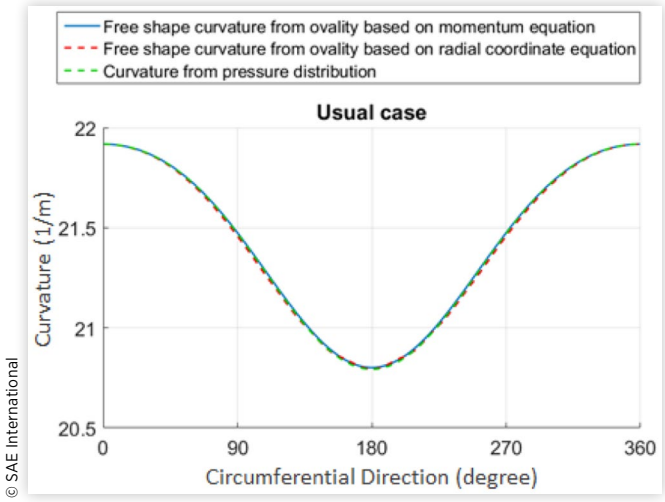

FIGURE 11 Free shape curvature comparison (TC case).

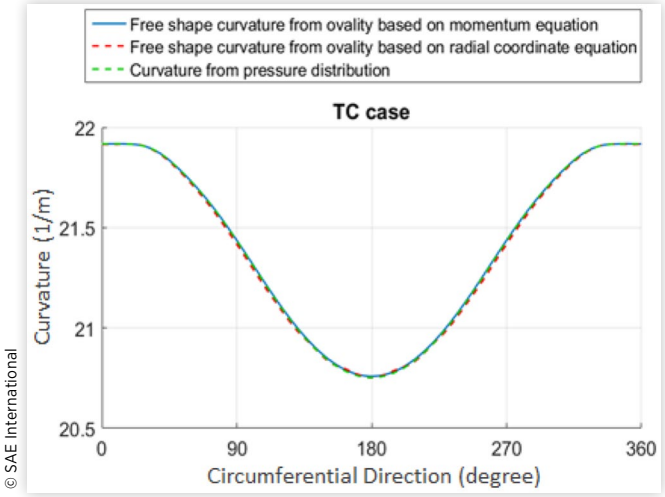

FIGURE 12 Force distribution comparison (Usual case). Red circles represent the points at the nodes of the elements considered.

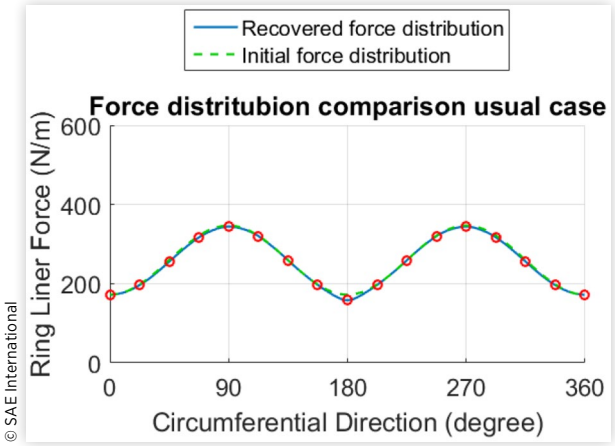

FIGURE 13 Force distribution comparison (TC case). Red circles represent the points at the nodes of the elements considered.

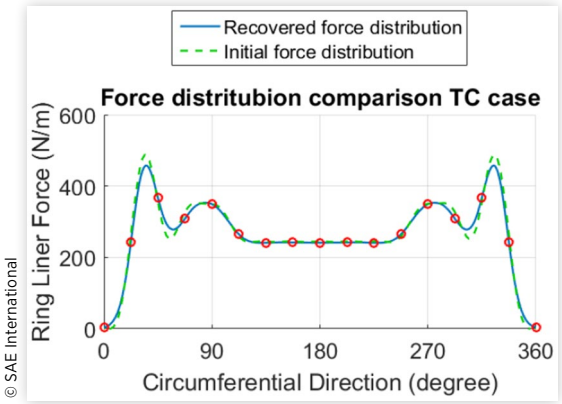

Validation of the Model Using Closed Shape Within a Flexible Band Measurement

Besides the theoretical force distribution, Mahle provided us with measured closed shape within a flexible band for the usual and the TC cases that has been used in Tomanik's work [15]. In this section we will present the results obtained from our model using these experimental data sets. The first sub part will be devoted to the description of the data processing procedure and the second one contains the obtained results.

Closed Shape Within a Flexible Band Data Processing

The closed shape within a flexible band measurement is carried out using a stylus-based equipment. We carry out the data processing by approximating the measures with the 5^{th} order polynomial shape functions. We carry out the interpolation using the least square method and we impose the continuity of the third derivatives at the nodes belonging to two elements (i.e. all nodes except the two corresponding to the ring tips). The measured and fitted closed shape for the two cases are plotted in Figures 14 and 15. The average difference between the measures and their fit is in the order of $10^{-10}m$. More details can be found in M.A. Bhouri thesis [19].

FIGURE 14 Fitted measured closed shape in centralized representation (Usual case).

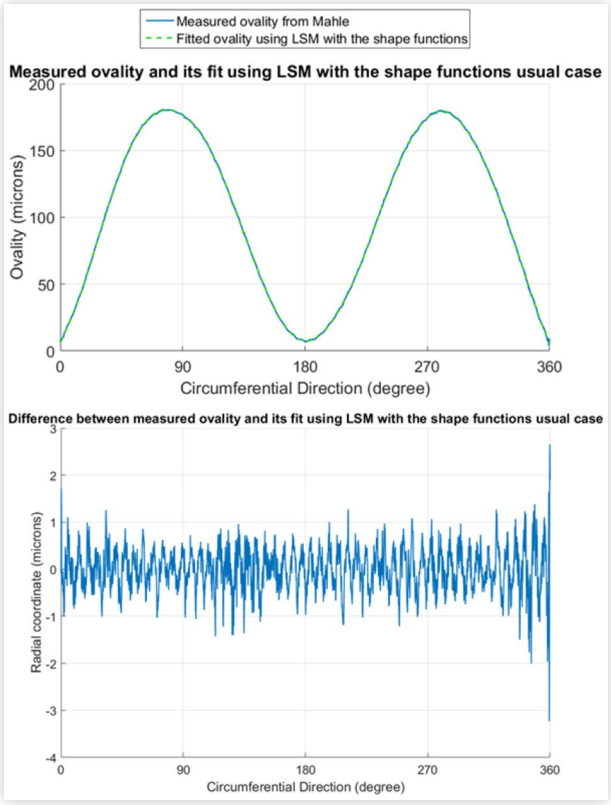

FIGURE 15 Fitted measured closed shape in centralized representation (TC case).

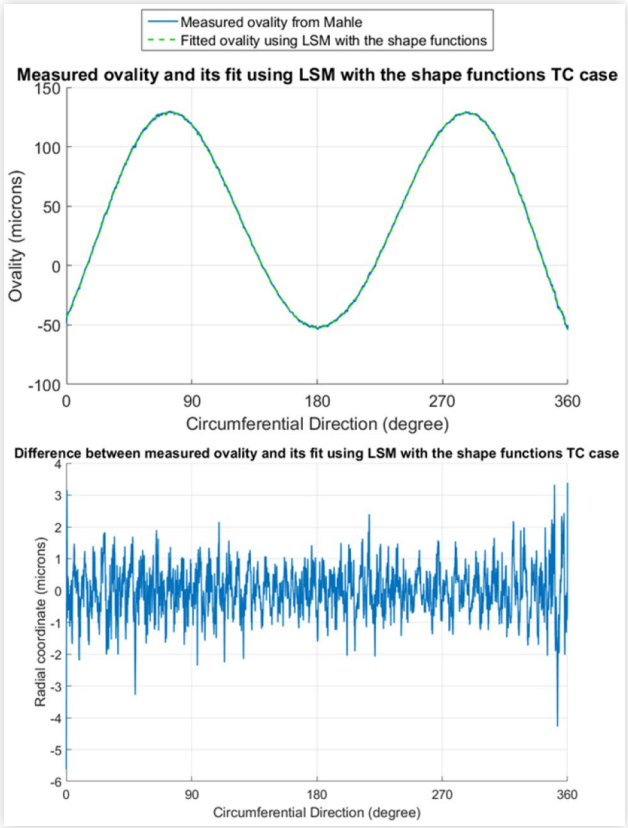

Once we have our fitted data in the centralized representation, we convert it to the usual one and use our sub-models to recover the ring free shape and the force distribution for the closed circular shape. The corresponding results are presented in the following section.

Results

Using the sub model - Determining ring's closed shape within a flexible band using its free shape - we obtain the ring free shape and its curvature. Figures 16 and 17 present the results for the usual case while Figures 18 and 19 show the outputs for the TC case. We conclude that we are still able to recover the right free shape even when using the closed shape measures. The maximum relative error has slightly increased compared to the free shape computed from the theoretical closed shape distribution in the theoretical validation of the model since it goes from 0.6% to 0.7%.

The following graphs Figure 20 and 21 show the results obtained for the free shape curvatures. We observe that the difference between the free shape curvature obtained from the theoretical force distribution used in the theoretical validation of the model and the curvatures computed from the measured closed shape within a flexible band distribution is

FIGURE 16 Comparison of free shape obtained from theoretical force distribution and from measured closed shape within a flexible band in usual representation (usual case).

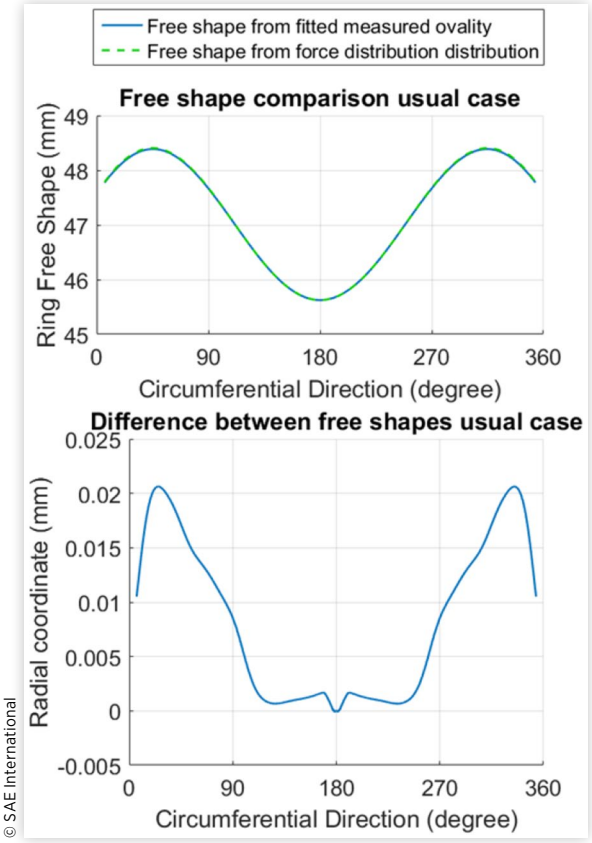

FIGURE 17 Comparison of free shape obtained from theoretical force distribution and from measured closed shape within a flexible band in radial plots (usual case).

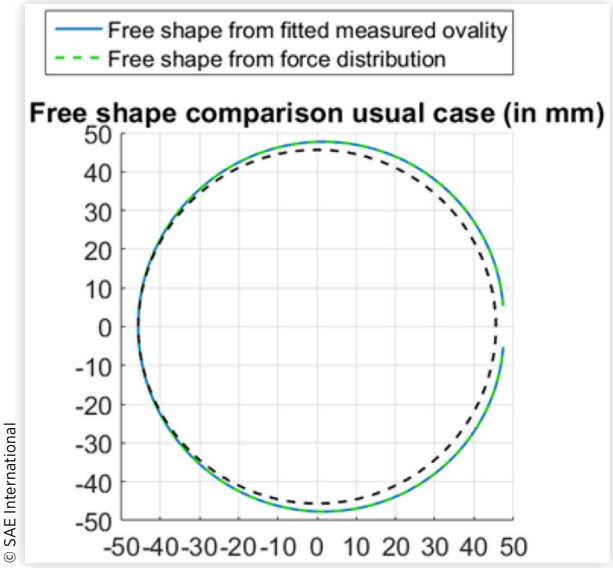

FIGURE 18 Comparison of free shape obtained from theoretical force distribution and from measured closed shape within a flexible band in usual representation (TC case).

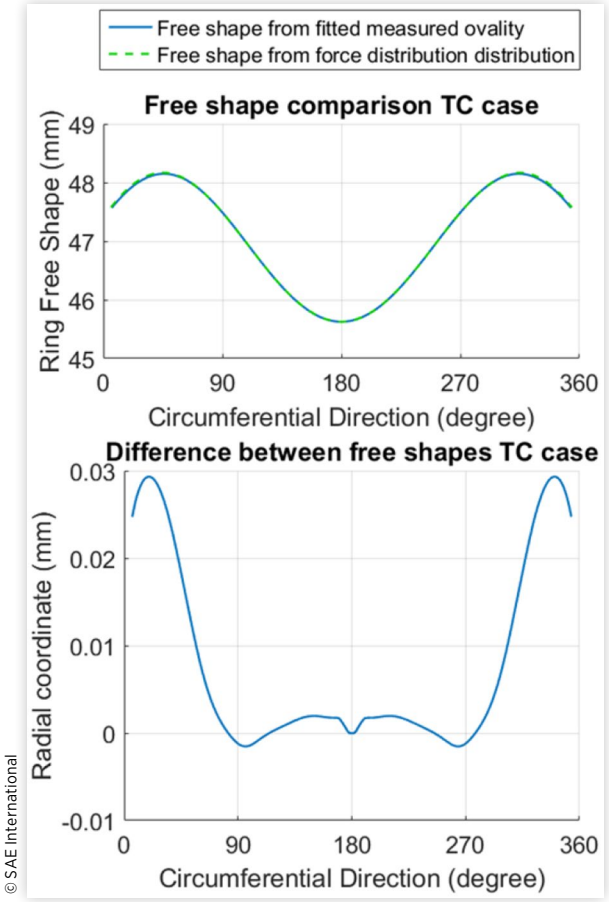

FIGURE 19 Comparison of free shape obtained from theoretical force distribution and from measured closed shape within a flexible band in radial plots (TC case).

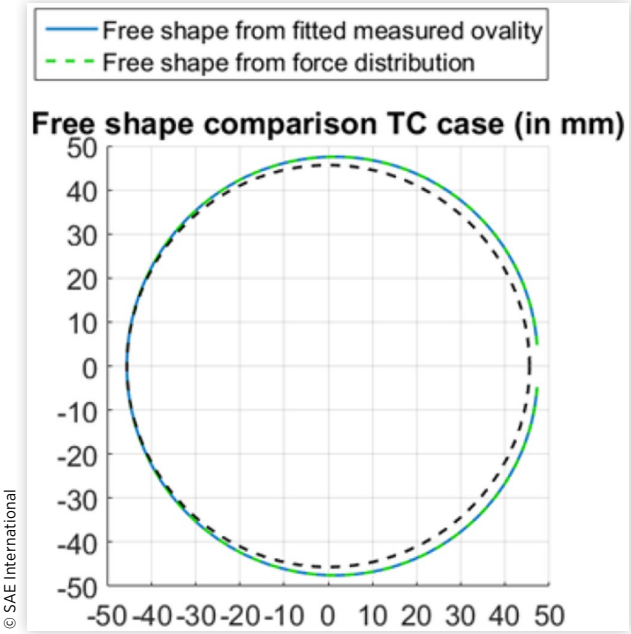

FIGURE 20 Free shape curvature comparison for measured closed shape within a flexible band (Usual case)

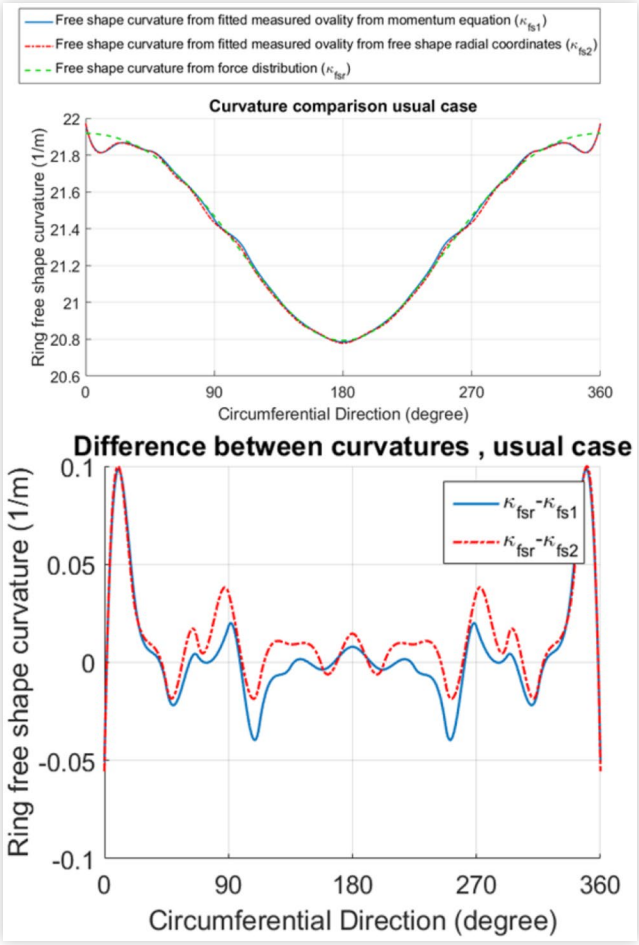

FIGURE 21 Free shape curvature comparison for measured closed shape within a flexible band (TC case)

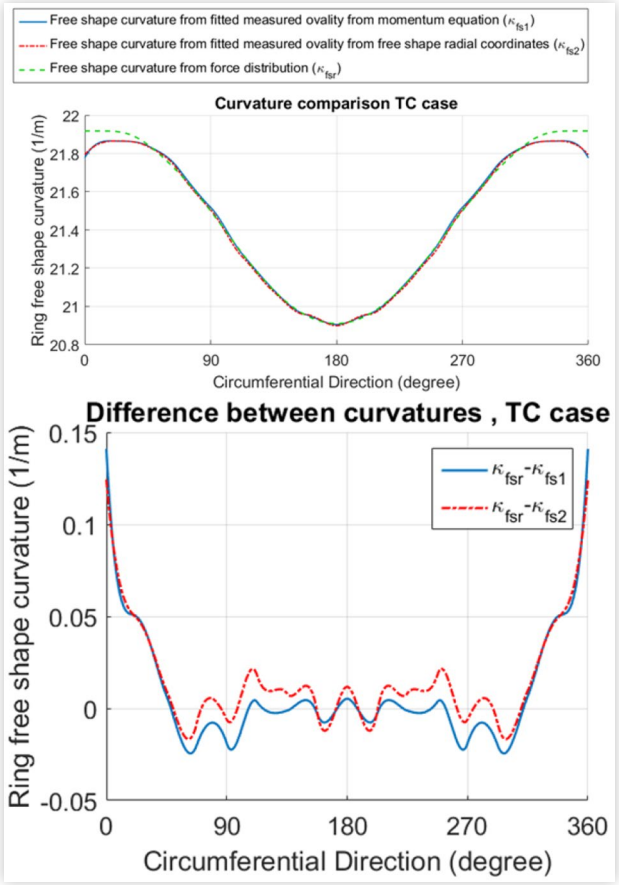

much more significant than the difference observed in the free shape. Indeed, the maximum relative error goes from 0.02% to 0.46% for the usual case regarding the curvature computed from the momentum equation and from 0.03% to 0.49 % for the TC case.

We explain these discrepancies by two factors. First, the fitted closed shape distribution and the one obtained in the theoretical validation of the model from the theoretical force distribution that lets us recover the right curvature and thus the force distribution, are off by $\pm 8\,\mu m$ for the usual case and $\pm 9\ \mu m$ for the TC one as we can see in Figure 22 and 23. This is well coherent with the radial distances deviation reported by Mahle. The modes observed in these differences correspond to low frequencies while the white noise filtered by our least square method presents high frequencies as we observed in Figures 14 and 15. We also notice that the white noise presents comparable amplitudes to the modes corresponding to the differences observed between the fitted closed shape distribution and the one giving the right free shape and force distribution. We also verified our data fitting by adding the difference between the closed shape distribution measurement and its fit to the closed shape distribution computed from the theoretical force distribution (the closed shape that gives back the right free shape and force distribution) and then processing that artificial closed shape distribution by fitting it and using

FIGURE 22 Difference between fitted measured closed shape within a flexible band and closed shape that recovers the right free shape and force distribution (usual case).

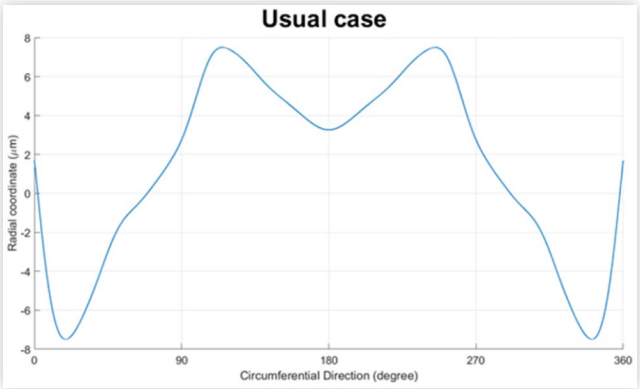

it as an input to our model. For both cases (Usual and TC) we were able to recover the exact free shape and force distributions.

The second reason that may explain the discrepancies observed is that even if the fitted closed shape within a flexible band distribution is still a good approximation within the deviation observed, its first and second derivatives should also be comparable to those of the right closed shape distribution. Indeed, the free shape curvature depends directly on the closed shape one based on the momentum equation (4) and

FIGURE 23 Difference between fitted measured closed shape within a flexible band and closed shape that recovers the right free shape and force distribution (TC case).

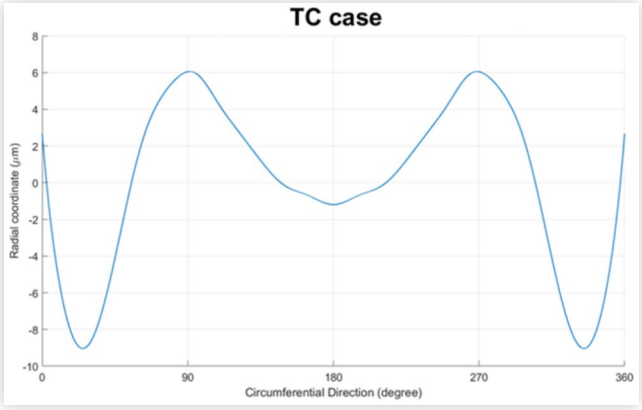

FIGURE 24 Comparison of 1st and 2nd derivatives of fitted measured closed shape within a flexible band and of the closed shape that recovers the right free shape and force distribution in usual representation (usual case).

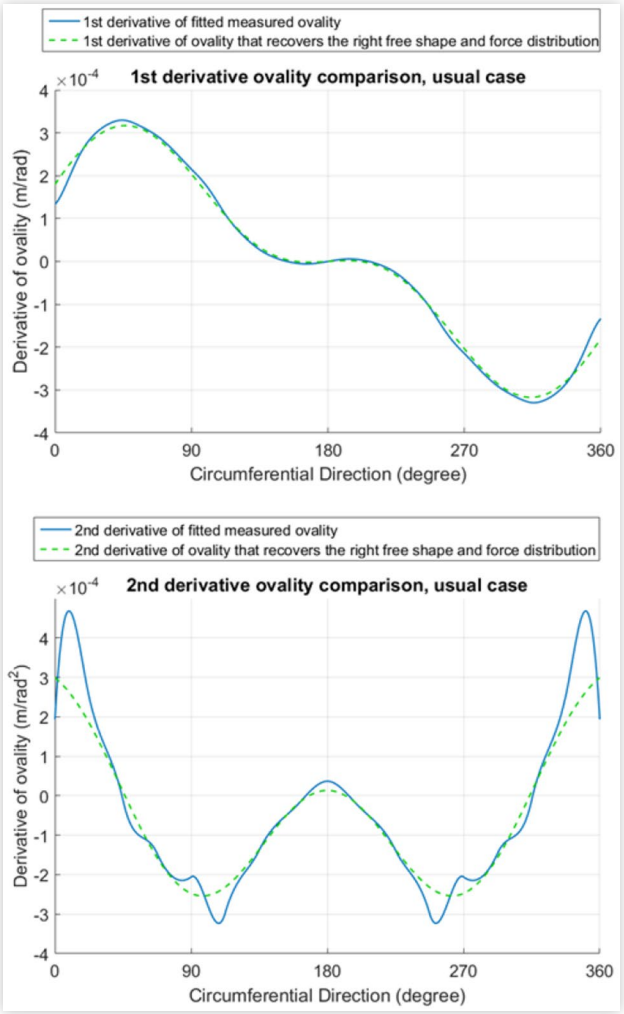

FIGURE 25 Comparison of 1st and 2nd derivatives of fitted measured closed shape within a flexible band and of the closed shape that recovers the right free shape and force distribution in usual representation (TC case).

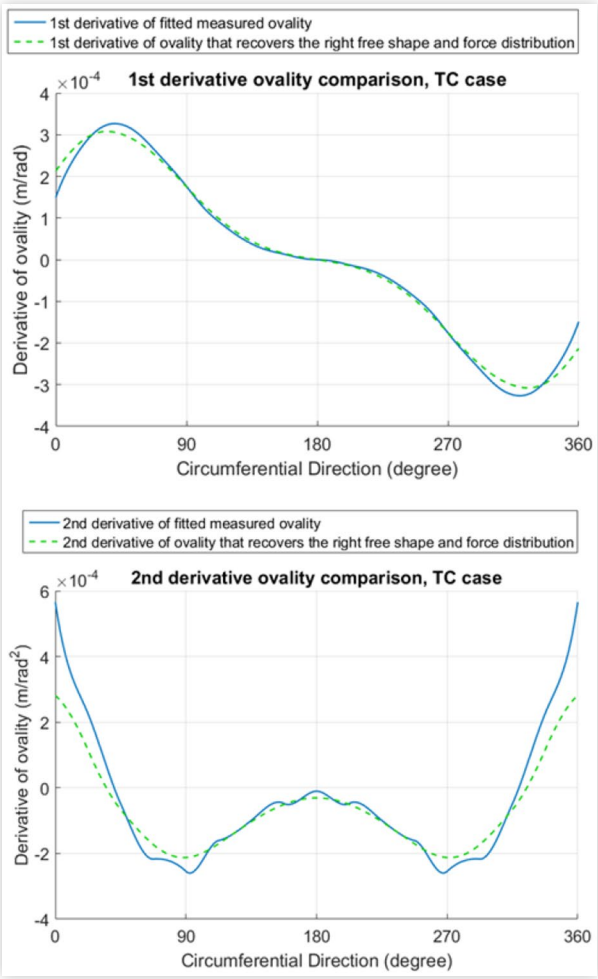

the closed shape curvature is a function of the radial displacement and its first and second derivatives. Figures 24 and 25 confirm the fact that even though the first derivative of the fitted closed shape within a flexible band distribution seems to be a fairly good approximation of the exact one, its second derivative presents a more significant deviation from the ideal second derivative distribution, both for the usual and the TC case. Using the curvatures computed from the fitted closed shape within a flexible band distribution we were not able to recover the force distribution in closed circular shape.

Finally, we study the sensitivity of our model to the noise level and to the number of "measuring points". This was carried out to find out how many points are needed to be measured and to look at the sensitivity of our model to the measuring error. The reason to try this was to verify if using less points would make our model less sensitive to the measurement error.

First we looked at the errors obtained for the recovered free shape coordinate, free shape curvature and radial force distributions by considering different number of points from the closed shape within a flexible band distribution that

FIGURE 35 Free shape coordinate and curvature distribution errors for different numbers of closed shape measuring points (Usual and TC cases).

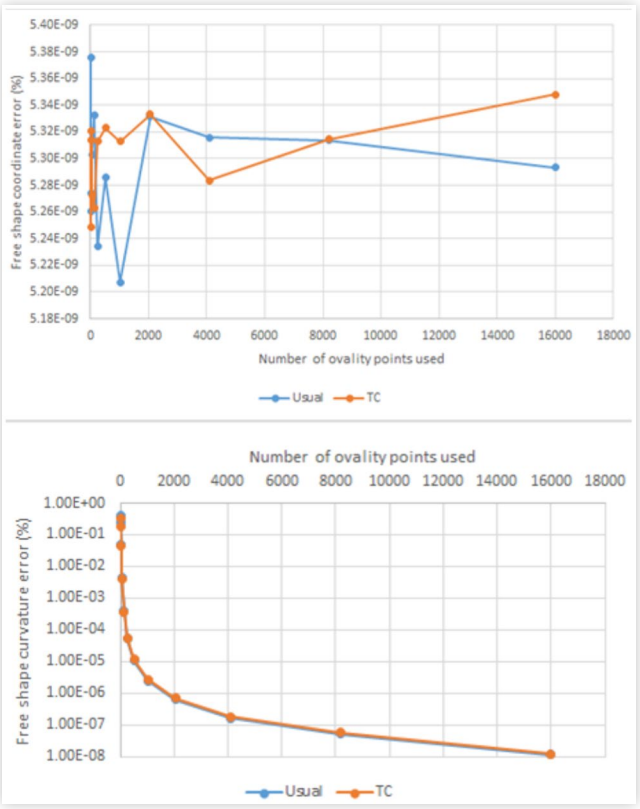

recovers the right force. For the force distribution, the error is defined as the average (over the distribution) of the relative error between the force distribution obtained by our model and the theoretical one. For the free shape coordinate and curvature, the errors are defined as average (over the distribution) of the relative error between the recovered distribution and the one that would give the exact force distribution. All the errors are given in percentage. As we can see in Figure 35, the free shape distribution recovered matches well the theoretical one even with only 9 points (smallest number of points considered) and the error does not decrease monotonously with the number of points considered. However, the curvature distribution does depend on that number and is accurate enough only when using at least 129 points (for Usual and TC case) as we can also see in Figure 36 giving the force distribution errors. Note that we obtained a high error for the recovered force distribution for the TC case. Indeed, this is related to the sharp variations of the theoretical distribution, which is confirmed by the deviations observed in the force distribution recovered from the theoretical one with a fine mesh (16001 points) as shown in Figure 13 unlike the better match obtained for the Usual case (Figure 12).

Then, for the Usual case and for different numbers of measuring points (513, 2049 and 16001), we artificially added the white noise filtered from Mahle measurements (bottom plot in Figure 14) to the theoretical closed shape within a flexible band distribution with different multiplication factors applied to the white noise (that we call Noise factor). The

FIGURE 36 Force distribution errors for different numbers of closed shape measuring points (Usual and TC cases).

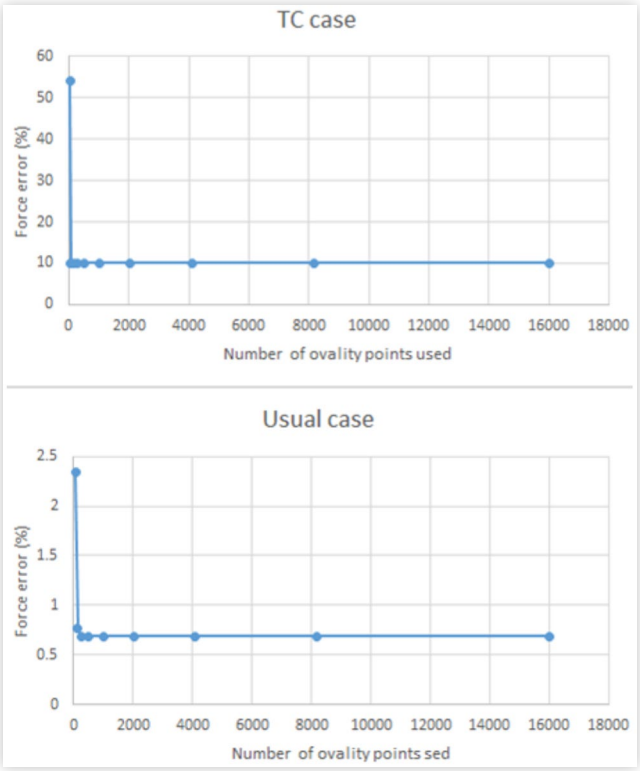

results are given in Figure 36. Using a bigger number of closed shape measuring points improves the accuracy of our model for any noise level. This shows that, despite the fact of having less points reduces the sensitivity to the measurement error, our model still needs a large enough data set (around 2000 measuring points) to reach a small enough error for the recovered force distribution and also to be robust to the noise level. Indeed, Mahle closed shape measurements include 3601 points which are not sufficient to give accurate results given that the experimental introduced error is larger than the artificial one we considered here. Therefore, this raises another point that could explain the reason why we could not recover the theoretical force distribution from the closed shape measurements.

Conclusion

We have developed a set of consistent models to relate the force in closed circular shape, the free shape and the closed shape within a flexible band distributions, which defines a complete tool that relates in any desired order these three ring's characterizations. The sub-model computing the free shape and force distribution using the closed shape within a flexible band one can consider any closed shape. A theoretical validation of these four models is presented by recovering the radial force distribution used first as an input and then recovered after being processed through all the four models.

We applied these models to measured closed shape within a flexible band by looking for the ring free shape and force

FIGURE 36 Force distribution, free shape coordinate and curvature errors for different numbers of closed shape within a flexible band measuring points and different noise factors (Usual case).

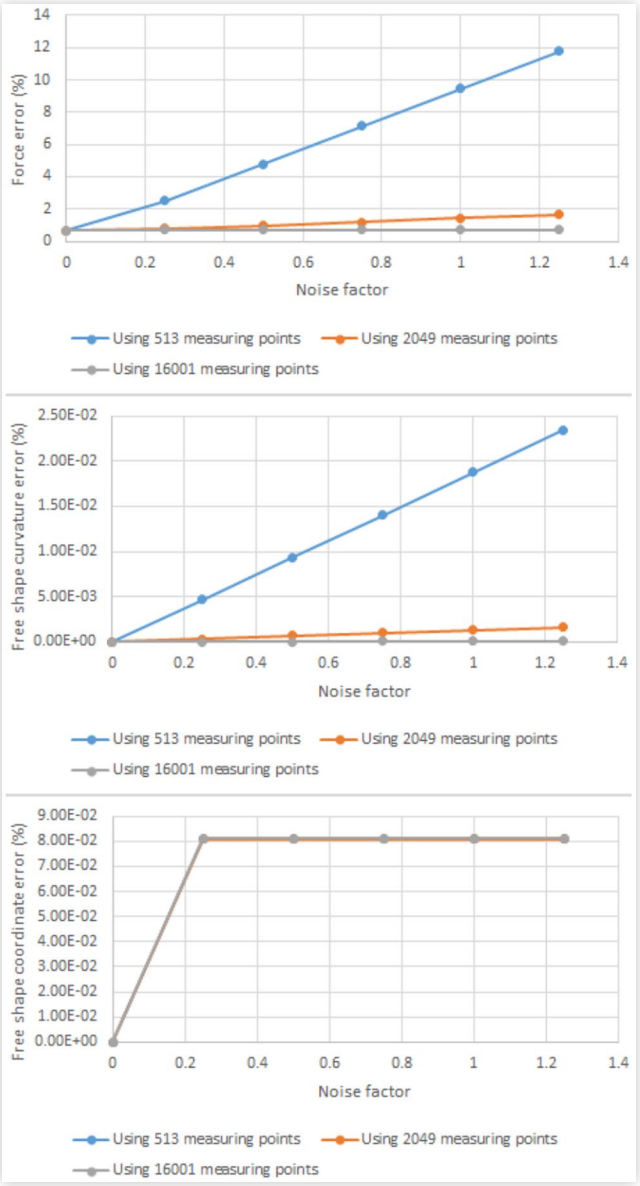

distribution. Fitting the measurement with a least square model based on the 3rd order polynomial shape functions used in our curved beam model lets us recover the ring free shapes properly for the two sets of data (Usual and TC). However, the free shape curvature that depends on the first and second derivative of the free shape radial coordinates was not close enough to the exact one that recovers the proper force distribution.

As shown previously, the deviations for measurement of the closed shape within a flexible band provided by Mahle explain well the difference obtained between the fitted closed shape and the theoretical one. This difference is large enough to make our model unable to recover the right force distribution. Apart from other fitting techniques for the measured closed shape within a flexible band, more measuring points, a statistical treatment for repeated measures carried on the same ring or a better experimental measurement process could be considered too. Besides, measurement related sources of error could be investigated further by considering more advanced and probably automated measurement techniques in the future like laser based ones to minimize human introduced deviations. Finally, we may also consider the influence of the friction when closing the ring. Indeed, computing the ring free shape based on the momentum equations (9) and (10) assumes that the force applied on the ring is locally normal as shown in Figure 4. Considering some friction models, even simple ones based on constant friction coefficient for instance, could give us an idea on the influence of the force tangential component on our results.

References

1. Tian, T., "Dynamic Behaviors of Piston Rings and Their Practical Impact. Part 1: Ring Flutter and Ring Collapse and Their Effects on Gas Flow and Oil Transport," *Proc IMechE, Part J: Journal of Engineering Tribology* 216(4):209-227, 2002, doi:10.1243/135065002760199961.
2. Tian, T., "Dynamic Behaviors of Piston Rings and Their Practical Impact. Part 2: Oil Transport, Friction, and Wear of Ring/Liner Interface and the Effects of Piston and Ring Dynamics," *Proc IMechE, Part J: Journal of Engineering Tribology* 216(4):229-247, 2002, doi:10.1243/135065002760199970.
3. English, C., "Kolbenringe," 2:64-65, 122-125, 270-277. In German.
4. Muller, R. "Calculation of the Shape and the Ovality of Rings Inside the Flexible Band Under Arbitrary Pressure", MTZ 32, 1971, in German.
5. Mierbach, A. "Calculation of the Pressure Distribution of Piston Rings based on their Shape", MTZ 55, 1994..
6. Ejakov, M.A., Schock, H.J., and Brombolich, L.J., "Modeling of Ring Twist For an IC Engine," SAE Technical Paper 982693, 1998.
7. Liu, L., Tian, T., and Rabuté, R., "Development and Applications of an Analytical Tool for Piston Ring Design," SAE Technical Paper 2003-01-3112, 2003, doi:10.4271/982693.
8. Liu, L. and Tian, T., "A Three-Dimensional Model for Piston Ring-Pack Dynamics and Blow-By Gas Flow," in ASME 2004 Internal Combustion Engine Division Fall Technical Conference ICEF2004-0968, 2004.
9. Liu, L. and Tian, T., "Modeling Piston Ring-Pack Lubrication With Consideration of Ring Structural Response," SAE Technical Paper 2005-01-1641, 2005, doi:10.4271/2005-01-1641.
10. Cheng, C., Kharazmi, A., and Schock, H., "Modeling of Piston Ring-Cylinder Bore-Piston Groove Contact," SAE Technical Paper 2015-01-1724, 2015, doi:10.4271/2015-01-1724.
11. Cheng, C., Kharazmi, A., Schock, H., Wineland, R., and Brombolich, L., "Three-Dimensional Piston Ring-Cylinder Bore Contact Modeling," *ASME. J. Eng. Gas Turbines Power.* 137(11):111505-111510, 2015, doi:10.1115/1.4030349.

12. Baelden, C., "A Multi-Scale Model for Piston Ring Dynamics, Lubrication and Oil Transport in Internal Combustion Engines," Ph.D. thesis, The Department of Mechanical Engineering, Massachusetts Institute of Technology, Cambridge, MA, 2014.
13. Baelden, C. and Tian, T., "A Dual Grid Curved Beam Finite Element Model of Piston Rings for Improved Contact Capabilities," *SAE Int. J. Engines* 7(1), 2014, doi:10.4271/2014-01-1085.
14. Liu, L., " Modeling the Performance of the Piston Ring-Pack with Consideration of Non-Axisymmetric Characteristics of the Power cylinder System in Internal Combustion Engines," Ph.D. thesis, The Department of Mechanical Engineering, Massachusetts Institute of Technology, Cambridge, MA, 2005.
15. Tomanik, E. and Bruno, R., "Calculation of Piston Ring Radial Pressure Distribution from its Measured Free Shape," SAE Technical Paper 2012-01-1322, 2012, doi:10.4271/2012-01-1322.
16. Liu, Y., "A Multi-scale Model Integrating both Global Ring Pack Behavior and Local Oil Transport in Internal Combustion Engines," Ph.D. thesis, The Department of Mechanical Engineering, Massachusetts Institute of Technology, Cambridge, MA, 2017.
17. Liu, Y. and Tian, T., "Development and Application of Ring-Pack Model Integrating Global and Local Processes. Part 1: Gas Pressure and Dynamic Behavior of Piston Ring Pack," *SAE Int. J. Engines* 10(4), 2017, doi:10.4271/2017-01-1043.
18. Liu, Y., Li, Y., and Tian, T., "Development and Application of Ring-Pack Model Integrating Global and Local Processes. Part 2: Ring-Liner Lubrication," *SAE Int. J. Engines* 10(4), 2017, doi:10.4271/2017-01-1047.
19. Bhouri, M.A., "Curved beam based model for piston-ring designs in internal combustion engines," M.S. thesis, The Department of Mechanical Engineering, Massachusetts Institute of Technology, Cambridge, MA, 2017.

Acknowledgments

This work has been sponsored by the MIT consortium on Lubrication in Internal Combustion Engines with additional support from Argonne National Laboratory and the US Department of Energy. The authors would like to thank all current members: Daimler AG, Mahle GmbH, MTU Friedrichshafen, PSA Peugeot Citroën, Renault S.A., Royal Dutch Shell, Toyota, Volkswagen AG, Volvo Cars, Volvo Truck, and Weichai Power.

ISSN 0148-7191